β equilibrium in neutron-star mergers

Mark G. Alford and Steven P. Harris

Physics Department, Washington University, St. Louis, Missouri 63130, USA

We show that the commonly used criterion for β equilibrium in neutrino-transparent dense nuclear matter becomes invalid as temperatures rise above 1 MeV. Such temperatures are attained in neutron-star mergers. By numerically computing the relevant weak-interaction rates we find that the correct criterion for β equilibrium requires an isospin chemical potential that can be as large as 10–20 MeV, depending on the temperature at which neutrinos become trapped.

I. INTRODUCTION

β-equilibrated nuclear matter is of great physical significance as the main constituent of neutron stars. It is therefore important to establish the conditions for β equilibrium at the densities and temperatures that are astrophysically relevant.

In this paper we point out that the standard low-temperature criterion for β equilibrium in neutrino-transparent nuclear matter is not valid at temperatures and densities that are attained in neutron-star mergers. After their formation in a supernova, neutron stars quickly cool [1–3] below a temperature of 1 MeV, but neutron-star mergers (now observed [4,5]) contain nuclear matter at densities above nuclear saturation density n_{sat} and temperatures ranging up to 30 MeV [6–11]. The proper way to treat nuclear matter in mergers is to do a full neutrino transport calculation. However, this is a technically formidable task, so many treatments (see, e.g., Refs. [11–15]) assume neutrino transparency up to some temperature T_{trap}, using a cold neutrinoless β-equilibrated equation of state for $T < T_{trap}$. In this work we provide the leading finite-temperature corrections to the β equilibration condition in neutrino-transparent matter. We find that β equilibrium requires an isospin chemical potential that increases with the temperature T, reaching a few MeV at $T \approx 1$ MeV and rising to almost 25 MeV at $T \approx 10$ MeV. Since the neutron stars start the merger process in a state of high density but low temperature, and then heat up as the merger proceeds, we expect that there will be regions in which neutrinos are not trapped and the temperature and density are in the range where our predicted corrections are significant. The size of such ranges is not yet clear because current estimates of the neutrino mean-free path depend on the energy of the neutrinos and on the assumptions about nuclear matter [16–19]. In Appendix A we summarize a recent calculation of the mean-free path of neutrinos, indicating that neutrinos are not trapped until temperatures rise above approximately 5 MeV.

We work in natural units, where $\hbar = c = k_B = 1$. All data presented in our figures can be found in the Supplemental Material [20].

A. The Fermi-surface approximation

Neutron stars contain nuclear matter at temperatures that are much smaller than the Fermi energy of the nucleons and electrons. Neutron stars are finite-size systems so we also have to take into account finite-size effects such as neutrino transparency, which occurs at temperatures low enough so that the neutrino mean-free path is larger than the size of the star [16,18,21,22]. At high enough density, flavor equilibration occurs via direct Urca processes (neutron decay and electron capture):

$$n \rightarrow p + e^- + \bar{\nu}_e, \quad p + e^- \rightarrow n + \nu_e. \quad (1)$$

Note that, because neutrinos escape from the star, neutrinos can only occur in the final state.

In the $T \rightarrow 0$ limit, one can work in the "Fermi-surface (FS) approximation" where the Urca processes are dominated by nucleons and electrons close to their Fermi surfaces. In the Fermi-surface approximation, the criterion for β equilibrium in nuclear matter is

$$\mu_n = \mu_p + \mu_e, \quad (2)$$

which can be obtained by ignoring the neutrinos in the Urca process and thinking of the Urca reactions as $n \leftrightarrow p + e^-$, in which case the principle of detailed balance tells us that Eq. (2) is the condition for equilibrium. Here μ_n, μ_p, and μ_e are the relativistic chemical potentials (i.e., including the rest mass) of the neutron, proton, and electron, respectively.

In the Fermi-surface approximation there is a threshold density above which the direct Urca processes shown in Eq. (1) are dominant. Below that threshold they are kinematically forbidden, and equilibration occurs via modified Urca processes which involve an additional spectator nucleon in the initial and final state [22–24].

In this paper, we consider only the six Urca processes (two direct and four modified) where the charged lepton involved is an electron. Weak interactions involving positrons are negligible, since the electron chemical potential is always above 100 MeV for the densities that we will consider, and so the positron occupation is suppressed by a factor of more than

$\exp(-100 \text{ MeV}/T)$. Additionally, for simplicity we neglect Urca processes involving muons, because even though those processes are not negligible, they do not qualitatively change the conclusions that we present here.

B. Breakdown of the Fermi-surface approximation

The β-equilibrium criterion (2) is not guaranteed to be valid under all circumstances because neutrinos are not in statistical equilibrium in systems that are neutrino transparent. Because neutrinos escape, they only occur in final states[1] so the two processes (1) whose rates have to balance are not exact inverses of each other, which means that the principle of detailed balance is not guaranteed to hold. (For a discussion in the context of hot plasmas see Refs. [25,26].) Detailed balance is a good approximation when neutrinos play a negligible role; namely, in the $T \to 0$ limit where the Fermi-surface approximation is valid. However, for astrophysical applications we need to know the criterion for β equilibration at a range of temperatures up to 30 MeV. We will now make a rough estimate of the temperature at which the corrections to Eq. (2) become significant. In Sec. IV we will perform a full calculation.

For densities below the direct Urca threshold we can estimate the range of validity of the Fermi-surface approximation by noting that it will become invalid when the exponential suppression of direct Urca processes involving particles away from their Fermi surface is not so severe as to make those processes negligible relative to modified Urca. In direct Urca processes the proton is expected to play a crucial role since it is the most nonrelativistic fermion, which means that the energy E_p of a proton rises very slowly as the momentum p_p of the proton deviates from its Fermi surface: $E_p - E_{F_p} \approx (p_p - p_{F_p})p_{F_p}/m_p$, where p_{F_p} is the Fermi momentum of the proton, E_{F_p} is the proton Fermi energy, and m_p is the proton mass. For particles on their Fermi surfaces, the momentum mismatch for direct Urca at densities around $3n_{\text{sat}}$ in nuclear matter described by the Akmal–Pandharipande–Ravenhall (APR) equation of state [27] is $p_{\text{miss}} = p_{Fn} - p_{Fp} - p_{Fe} \approx 50$ MeV (see, e.g., Fig. 2 in Ref. [28]), and the proton Fermi momentum is about 220 MeV. The energy cost of finding a proton that is p_{miss} from its Fermi surface is $p_{\text{miss}}p_{F_p}/m_p \approx 12$ MeV, so we might expect that direct Urca electron capture, where the probability of finding a proton from above its Fermi surface includes a Boltzmann factor, becomes unsuppressed at temperatures of order 10 MeV, and that it starts to compete with modified Urca at even lower temperatures.

In fact, as can be shown from the Urca rate expressions that we review in Sec. II, at $3n_{\text{sat}}$ the modified Urca rate is approximately a factor of $[m_n T/(3m_\pi^2)]^2$ smaller than the above-threshold direct Urca rate, where m_n and m_π are the neutron and pion masses, respectively. Thus, the below-

threshold direct Urca electron-capture rate would begin to compete with modified Urca when

$$e^{-(E_p - E_{F_p})/T} \approx \left(\frac{m_n T}{3m_\pi^2}\right)^2, \tag{3}$$

which, for a proton with $E_p - E_{F_p} = 12$ MeV, is when the temperature is between 1 and 2 MeV.

As we will show below in an explicit calculation, this is a fair estimate. The Fermi-surface approximation starts to become invalid at temperatures $T \gtrsim 1$ MeV which are still much less than the Fermi energies, and may still be low enough for neutrinos to escape from the star. This leads us to expect corrections to the low-temperature criterion (2) for β equilibrium at temperatures and densities that are relevant for neutron-star mergers, in which nuclear matter is heated to temperatures up to 30 MeV.

In Sec. II we reproduce the standard calculation of the rates of neutron decay and electron capture, which uses the Fermi-surface approximation. To describe nuclear matter we will use the APR equation of state [27].

In Sec. III we describe the kinematics of the below-threshold direct Urca process, and how particles away from their Fermi surface can participate in the processes, leading to exponential suppression of the direct Urca rates for temperatures below about 10 MeV.

In Sec. IV we describe the results of a numerical calculation of the rates which includes contributions from the whole phase space.

II. URCA PROCESSES IN THE FERMI-SURFACE APPROXIMATION

We now obtain the standard expressions for the rate of the direct and modified Urca processes in matter with the APR equation of state. We will assume ultrarelativistic electrons and neutrinos, but nucleons that are nonrelativistic, with dispersion relation

$$E_i = m_{\text{eff},i} + \frac{p_i^2}{2m_i}, \tag{4}$$

where, following Roberts *et al.* [19], at each density, $m_{\text{eff},i}$ is chosen such that the Fermi energy $E_{F,i} \equiv E_i(p_{F_i})$ matches the chemical potential μ_i from the APR equation of state, which is a simple way of taking into account the nuclear mean field. For the kinetic mass m_i we use the rest mass in vacuum.

A. Direct Urca

In the $T \to 0$ limit, the Fermi-surface approximation is valid and conservation of energy and momentum ensures that the direct Urca process (1) can only occur above the direct Urca threshold density where the triangle condition

$$p_{Fn} < p_{Fp} + p_{Fe}, \tag{5}$$

holds. For densities below the threshold density, the electron and proton Fermi momenta are not large enough to add up to the neutron Fermi momentum (the three momentum vectors cannot be made to form a triangle) and so the direct Urca reaction is prohibited. As density increases, the proton and

---

[1]The fact that neutrinos occur only in final states means that they are out of statistical equilibrium. This is different from being in statistical equilibrium with zero chemical potential, in which case there would be a thermal population of neutrinos which could occur in initial states as well.

electron Fermi momenta grow more quickly than the neutron Fermi momentum and when the threshold density is reached, they, when co-aligned, add up to exactly the neutron Fermi momentum. Above threshold, the proton and electron Fermi momenta can add up to the neutron Fermi momentum even when they are not co-aligned [22].

The rates of the two direct Urca processes are given by [22,29]

$$
\Gamma_{dU,nd} = \int \frac{d^3 p_n}{(2\pi)^3} \frac{d^3 p_p}{(2\pi)^3} \frac{d^3 p_e}{(2\pi)^3} \frac{d^3 p_\nu}{(2\pi)^3} \langle |\mathcal{M}|^2 \rangle (2\pi)^4
$$
$$
\times \delta^4(p_n - p_p - p_e - p_\nu) f_n (1 - f_p)(1 - f_e), \quad (6)
$$

$$
\Gamma_{dU,ec} = \int \frac{d^3 p_n}{(2\pi)^3} \frac{d^3 p_p}{(2\pi)^3} \frac{d^3 p_e}{(2\pi)^3} \frac{d^3 p_\nu}{(2\pi)^3} \langle |\mathcal{M}|^2 \rangle
$$
$$
\times (2\pi)^4 \delta^4(p_n - p_p - p_e + p_\nu)(1 - f_n) f_p f_e, \quad (7)
$$

where f_i are the Fermi–Dirac distributions for n, p, or e, and the matrix element is

$$
\langle |\mathcal{M}|^2 \rangle = 2G^2 \left[1 + 3g_A^2 + (1 - g_A^2) \frac{\mathbf{p}_e \cdot \mathbf{p}_\nu}{E_e E_\nu} \right], \quad (8)
$$

where $G^2 = G_F^2 \cos^2 \theta_c = 1.1 \times 10^{-22}$ MeV^{-4}, where G_F is the Fermi coupling constant and θ_C is the Cabibbo angle, and the axial-vector coupling constant $g_A = 1.26$. These rate integrals are evaluated in the Fermi-surface approximation, so we set $|\mathbf{p}_i| = p_{F_i}$ in all smooth functions of momentum in the integral, and the neutrino three-momentum is neglected. In this approximation we can perform phase-space decomposition, splitting the rate integral into an angular integral and an energy integral which can be straightforwardly evaluated, revealing that the direct Urca neutron decay and electron-capture rates are identical when Eq. (2) holds, and are given by [22,30,31]

$$
\Gamma_{dU,nd} = \Gamma_{dU,ec} = A_{dU} G^2 (1 + 3g_A^2) m_n m_p p_{Fe} \vartheta_{dU} T^5,
$$
$$
\vartheta_{dU} \equiv \begin{cases} 0 & \text{if } p_{Fn} > p_{Fp} + p_{Fe} \\ 1 & \text{if } p_{Fn} < p_{Fp} + p_{Fe}, \end{cases}
$$
$$
A_{dU} \equiv 3[\pi^2 \zeta(3) + 15\zeta(5)]/(16\pi^5) \approx 0.0170. \quad (9)
$$

B. Modified Urca

Below the direct Urca threshold density, modified Urca processes provide the leading contribution in the $T \to 0$ limit because, although they are suppressed by a higher power of T, they are kinematically allowed for particles on their Fermi surfaces. Using the Fermi-surface approximation and neglecting the neutrino three-momentum, we can perform phase-space decomposition and calculate the rates.

For the modified Urca processes, which involve strong interactions between the nucleons, we use the matrix elements given by Yakovlev *et al.* [22] and Friman and Maxwell [32], which involve a long-range one-pion exchange interaction. The matrix element for neutron decay and electron capture with a neutron spectator (n-spectator modified Urca) is given by

$$
\langle |\mathcal{M}_n|^2 \rangle = 84 G^2 \frac{f_{\pi NN}^4}{m_\pi^4} \frac{g_A^2}{E_e^2} \frac{p_{Fn}^4}{(p_{Fn}^2 + m_\pi^2)^2}, \quad (10)
$$

and the matrix element for neutron decay and electron capture with a proton spectator (p-spectator modified Urca) is given by

$$
\langle |\mathcal{M}_p|^2 \rangle = 96 G^2 \frac{f_{\pi NN}^4}{m_\pi^4} \frac{g_A^2}{E_e^2} \frac{(p_{Fn} - p_{Fp})^4}{\left[(p_{Fn} - p_{Fp})^2 + m_\pi^2\right]^2}, \quad (11)
$$

with the p-wave πN coupling constant $f_{\pi NN} \approx 1$.

When the traditional β-equilibrium condition (2) is used, the n-spectator modified Urca neutron decay and electron-capture rates are equal and given by [21,22,31,33]

$$
\Gamma_{mU,n} = A_{mU} G^2 f_{\pi NN}^4 g_A^2 \frac{m_n^3 m_p}{m_\pi^4} \frac{p_{Fn}^4 p_{Fp}}{(p_{Fn}^2 + m_\pi^2)^2} \vartheta_n T^7,
$$
$$
\vartheta_n \equiv \begin{cases} 1 & \text{if } p_{Fn} > p_{Fp} + p_{Fe} \\ 1 - \frac{3}{8} \frac{(p_{Fp} + p_{Fe} - p_{Fn})^2}{p_{Fp} p_{Fe}} & \text{if } p_{Fn} < p_{Fp} + p_{Fe}. \end{cases} \quad (12)
$$

See Sec. 6 of Ref. [31] for a comprehensive discussion of the integrals involved in the Fermi-surface approximation of the modified Urca rates, including clarification of errors and omissions in the literature.

The p-spectator modified Urca neutron-decay and electron-capture rates are equal to each other when Eq. (2) holds and are given by [21,22,31,33]

$$
\Gamma_{mU,p} = \frac{A_{mU}}{7} G^2 f_{\pi NN}^4 g_A^2 \frac{m_n m_p^3}{m_\pi^4} \frac{p_{Fn}(p_{Fn} - p_{Fp})^4}{\left[(p_{Fn} - p_{Fp})^2 + m_\pi^2\right]^2} \vartheta_p T^7,
$$
$$
\vartheta_p \equiv \begin{cases} 0 & \text{if } p_{Fn} > 3p_{Fp} + p_{Fe} \\ \frac{(3p_{Fp} + p_{Fe} - p_{Fn})^2}{p_{Fn} p_{Fe}} & \text{if } \begin{array}{l} p_{Fn} > 3p_{Fp} - p_{Fe} \\ p_{Fn} < 3p_{Fp} + p_{Fe} \end{array} \\ 4\frac{3p_{Fp} - p_{Fn}}{p_{Fn}} & \text{if } \begin{array}{l} 3p_{Fp} - p_{Fe} > p_{Fn} \\ p_{Fn} > p_{Fp} + p_{Fe} \end{array} \\ \left(2 + 3\frac{2p_{Fp} - p_{Fn}}{p_{Fe}} - 3\frac{(p_{Fp} - p_{Fe})^2}{p_{Fn} p_{Fe}}\right) & \text{if } p_{Fn} < p_{Fp} + p_{Fe} \end{cases}, \quad (13)
$$

where $A_{mU} \approx 7 \times 2300/(64\pi^9) \approx .0084$. We see that the p-spectator modified Urca process does have a threshold density, in this case the density where $p_{F_n} = 3p_{F_p} + p_{F_e}$, which occurs at a proton fraction $x_p = 1/65$. Thus, the p-spectator

modified Urca process is only prohibited at extremely low densities [22], well below nuclear saturation density, which is the minimum density that we consider here. In Appendix B, we give the Fermi-surface approximation for the modified Urca rates when Eq. (2) is violated by an amount $\xi = (\mu_n - \mu_p - \mu_e)/T$.

In the $T \to 0$ limit, where the Fermi-surface approximation is valid, the standard low-temperature β-equilibrium condition holds: when Eq. (2) is obeyed, the neutron-decay and electron-capture rates balance for both direct and modified Urca processes.

In the upper panels of Figs. 2 and 3, we have plotted, among other curves that we explain in Sec. IV, the Fermi-surface approximation of the two direct Urca (in dotted, green) and four modified Urca (labeled "mU," in blue) rates in APR matter for $T = 500$ keV and 5 MeV, respectively. For the APR equation of state the direct Urca threshold density is around $5n_{\text{sat}}$. Above threshold, the direct Urca neutron-decay and electron-capture rates are identical and dominate over the modified Urca processes which have no threshold in the density range we consider. Below threshold, neither direct Urca process is allowed and so the four modified Urca processes dominate. The two n-spectator modified Urca processes are slightly more important than the two p-spectator modified Urca processes. As long as the Fermi-surface approximation is used, and Eq. (2) is imposed, the proton-producing Urca processes balance the neutron-producing Urca processes exactly at all densities and temperatures.

III. URCA PROCESSES BEYOND THE FERMI-SURFACE APPROXIMATION

A. Particles away from their Fermi surface

To discuss the rates it is useful to introduce the concept of the single-particle free energy, defined as $\gamma_i(p) \equiv E_i(p) - \mu_i = E_i(p) - E_{F,i}$ [see Eq. (4) and the subsequent discussion]. The single-particle free energy tells us how far in energy a given state is from its Fermi surface.

At densities below the threshold density, the direct Urca process becomes Boltzmann suppressed because, after imposing energy and momentum conservation, the phase-space integral is dominated by processes whose initial state includes particles above their Fermi surface or whose final state requires holes below their Fermi surface. In both cases the Fermi–Dirac factors in the rate expression provide a suppression factor of $\exp(-|\gamma_i|/T)$.

To see how strong the resultant Boltzmann suppression will be, we show in Fig. 1 the typical single-particle free energy γ_i for the particles participating in neutron decay (left panel) and electron capture (right panel) at various densities of nuclear matter described by the APR equation of state, and obeying the low-temperature criterion for β equilibration (2). To obtain the typical momenta and energies at a given density we impose energy and momentum conservation to reduce the momentum space integral to the lowest possible dimension and find the point at which the product of Fermi–Dirac factors attains its maximum value. We emphasize that these typical momenta and energies are independent of temperature.
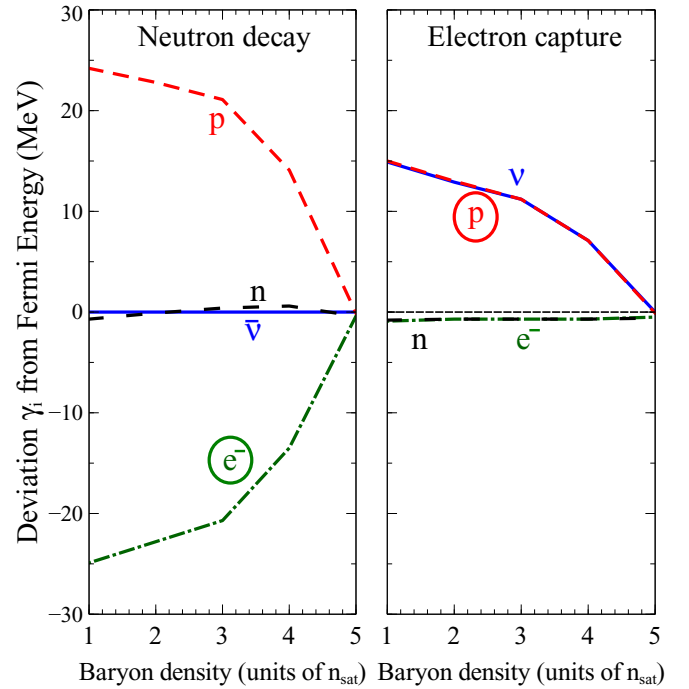

FIG. 1. Energy relative to their Fermi energy (defined as "γ") for particles participating in direct Urca reactions in APR nuclear matter obeying the standard low-temperature condition (2) for β equilibrium. At each density we choose the momenta and energies of participating particles (consistent with energy and momentum conservation) that maximize the product of their Fermi–Dirac factors. Above threshold, all particles can have $\gamma = 0$. Below threshold, the plot shows the least-Boltzmann-suppressed processes. The circles indicate the particles that cause the Boltzmann suppression.

Temperature merely influences the strength of the Boltzmann suppression due to particles with finite single-particle free energies γ_i participating in Urca reactions.

Above the direct Urca threshold density (about $5n_{\text{sat}}$ for the APR equation of state) we find, as expected, that particles on their Fermi surface (i.e., with $\gamma = 0$) can participate in direct Urca processes while conserving energy and momentum. Below the direct Urca threshold density, however, this is no longer true.

B. Below-threshold direct Urca neutron decay

For direct Urca neutron decay, the kinematic obstacle is that although a neutron on its Fermi surface has the same free energy as a proton on its Fermi surface and an electron on its Fermi surface (they all have $\gamma = 0$), the neutron's momentum is larger than the co-linear sum of the proton and electron momenta. We see in Fig. 1 (left panel) that the best available option below threshold is for a neutron on its Fermi surface to decay into a proton that is above its Fermi surface by an amount γ_p and an electron that is below its Fermi surface by the same amount, $\gamma_e = -\gamma_p$. The energies of the proton and electron still add up to the energy of the neutron, but a co-linear proton and electron now have more momentum then when they were both on their Fermi surfaces

because the proton's momentum rises rapidly as γ_p becomes more positive (because the proton is nonrelativistic with a low Fermi velocity) whereas the electron's momentum drops more slowly as γ_e becomes more negative, because the electron is relativistic. This "best available option" has a Boltzmann suppression factor of $\exp(-|\gamma_e|/T)$ because the final-state electron is trying to occupy a state in the already mostly occupied electron Fermi sea. From Fig. 1 we see that for the APR equation of state the value of $|\gamma_e|$ for this process is around 20 to 25 MeV at lower densities and then drops quickly to zero as we approach the direct Urca threshold.

C. Below-threshold direct Urca electron capture

For direct Urca electron capture, the kinematic obstacle is that a proton on its Fermi surface combined with an electron on its Fermi surface does not have enough momentum to produce a neutron on its Fermi surface. We see in Fig. 1 (right panel) that the best available option below threshold is for a proton above its Fermi surface to combine with an electron at its Fermi surface. Because the proton is nonrelativistic, this combination has enough momentum to create a neutron on its Fermi surface, and the excess energy γ_p (and the remaining momentum) goes into the final-state neutrino. This process has a Boltzmann suppression factor of $\exp(-|\gamma_p|/T)$ because we are unlikely to find initial-state protons far above the proton Fermi surface. From Fig. 1 we see that, for the APR equation of state, the value of $|\gamma_p|$ for this process is around 10 to 15 MeV at lower densities and then drops to zero as we approach the direct Urca threshold. The suppression is less than for neutron decay because the neutrino momentum can be directed opposite to the neutron momentum, so it helps to reduce the amount by which the proton needs to be above its Fermi surface.

D. Relevance of below-threshold direct Urca

We learn from the calculation presented in Fig. 1 that, below the threshold density, direct Urca processes are Boltzmann suppressed by a factor $\exp(-\gamma/T)$ where γ is in the 10 to 20 MeV range at lower densities, dropping to zero as the threshold is approached. For typical neutron-star temperatures $T \lesssim 0.1$ MeV the Boltzmann suppression is overwhelming, and direct Urca processes can be safely neglected compared with modified Urca. However, as we will show in the next section, at the temperatures characteristic of neutron-star mergers, this is not the case.

We note that a similar analysis of the Fermi–Dirac factors can be done with the modified Urca process, but it simply reproduces the expected finding that, at any density, the dominant contribution comes from particles close to their Fermi surfaces, so the Fermi-surface approximation is always valid for modified Urca and there is never any Boltzmann suppression of the rate.

In Sec. I, we estimated that, at densities below the direct Urca threshold, the Boltzmann-suppressed direct Urca electron-capture rate would match the modified Urca rate once the temperature rose to around 1 or 2 MeV. As we will see in the next section, a full calculation confirms this

estimate, showing that at $T \gtrsim 1$ MeV the contribution of below-threshold direct Urca processes leads to corrections to the low-temperature criterion for β equilibrium. Since the dominant contribution to the below-threshold direct Urca rates comes from particles that are far from their Fermi surfaces, we now calculate the direct Urca rates exactly, performing the entire momentum space integral.

IV. EXACT DIRECT URCA CALCULATION

Instead of assuming that all particles lie on their Fermi surfaces, we numerically evaluate the direct Urca rate integrals (6) and (7) with nonrelativistic nucleons, but without any further approximation, allowing the particles to have any set of momenta that is consistent with energy-momentum conservation. The details of the calculation, which reduces to a three-dimensional numerical integral, are given in Appendix C.

A. Urca rates

Figures 2 and 3 show in their upper panels the rates of various Urca processes in APR nuclear matter that obeys the low-temperature β-equilibrium criterion (2). As we will see, at $T \gtrsim 1$ MeV the Fermi-surface approximation starts breaking down and Eq. (2) is no longer the correct criterion for β equilibrium: an additional isospin-coupled chemical potential is needed to achieve β equilibrium, and its magnitude μ_δ is shown in the lower panel.

In Fig. 2, we see that, at a temperature of 500 keV, the Fermi-surface approximation is reasonably accurate. Well above the direct Urca threshold density the neutron decay and electron-capture rates are almost identical and agree well with the Fermi-surface approximation, so that when the low-temperature β-equilibrium criterion (2) is obeyed the net rate of neutron or proton creation is zero. Consequently, to the accuracy of our calculation (μ_δ is accurate to about ± 150 keV, described in Sec. IV B) there is no need for any additional isospin chemical potential to enforce β equilibrium. As the density drops below the threshold value, the direct Urca rates drop below the modified Urca rate and become negligible, and the modified Urca rates for neutron decay and electron capture are identical so again there is no net creation of neutrons or protons, and no noticeable modification to the low-temperature β-equilibrium criterion. However, it is interesting to note that below (and even slightly above) threshold the direct Urca rates for neutron decay and electron capture are not the same. The deviation increases as the density goes further below threshold. The size of the discrepancy agrees with our analysis in Fig. 1, where we determine the exponential suppression of each direct Urca rate, due to the Fermi–Dirac factors. Only right below threshold is there a region where the two direct Urca rates are different, but both are larger than the modified Urca rates, requiring a finite but small μ_δ to establish true β equilibrium. As temperature decreases further, this effect will vanish, and the low-temperature β-equilibrium criterion (2) will be increasingly valid.

In Fig. 3 we see that when we increase the temperature to $T = 5$ MeV the Fermi-surface approximation becomes
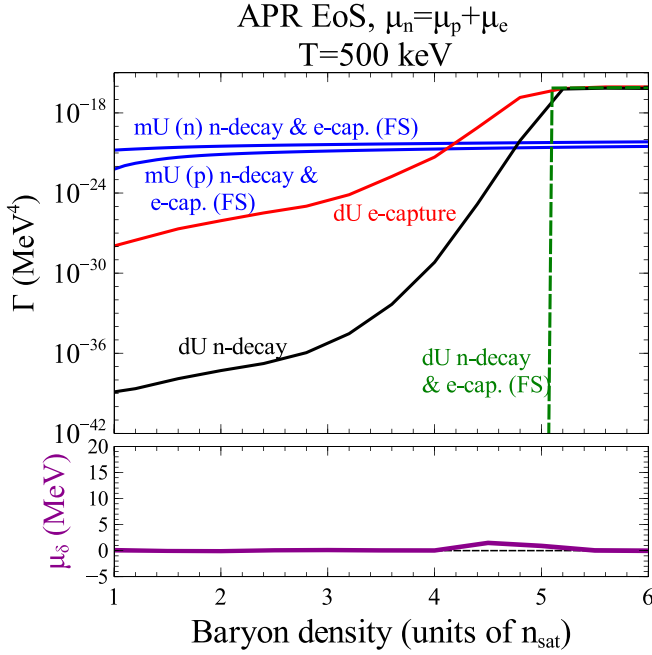
FIG. 2. Exact direct Urca and approximate modified Urca rates at $T = 500$ keV, obeying the low-temperature β-equilibrium condition (2). Above threshold, the two direct Urca rates balance each other, and they also match the approximate direct Urca rate. Below threshold, the direct Urca rates exponentially fall off, and modified Urca dominates. However, the two direct Urca rates have different exponential falloffs below threshold. In the lower plot, the deviation μ_δ from low-temperature β equilibrium needed to achieve true β equilibrium is plotted as a function of density.

FIG. 3. Exact direct Urca and approximate modified Urca rates at $T = 5$ MeV, obeying the low-temperature β-equilibrium condition (2). Above threshold, electron-capture direct Urca dominates and agrees with the approximate direct Urca rate calculation. At densities greater than $6n_{\text{sat}}$, we expect neutron decay direct Urca to match electron-capture direct Urca. Below threshold, electron-capture direct Urca dominates over all modified Urca processes, which contradicts the conventional wisdom. In the lower plot, the deviation μ_δ from low-temperature β equilibrium needed to achieve true β equilibrium is plotted as a function of density.

unreliable. The direct Urca electron-capture rate agrees with the Fermi-surface result above threshold, but it also shows no suppression below threshold, dominating over modified Urca and direct Urca neutron decay at all densities for which APR is well defined. This means that, when $\mu_n = \mu_p + \mu_e$ [Eq. (2)], there is a nonzero net rate of proton-to-neutron conversion, implying that the system is not in β equilibrium.

B. Full criterion for β equilibrium

The fact that electron capture is much less suppressed than neutron decay at $T \gtrsim 1$ MeV means that the system will be driven away from the state that obeys the standard low-temperature β-equilibrium criterion. The predominance of electron capture drives the neutron Fermi energy up and the proton Fermi energy down, effectively introducing an additional chemical potential that couples to the third component of isospin.

The general criterion for β equilibrium is

$$\mu_n = \mu_p + \mu_e + \mu_\delta, \qquad (13)$$

where $\mu_\delta = -\mu_I$ where μ_I is the chemical potential that couples to isospin, normalized according to a convention [34] where the proton has isospin $+1/2$ and the neutron has isospin $-1/2$.

As the proton density drops, the rates of electron capture and neutron decay move towards each other and eventually
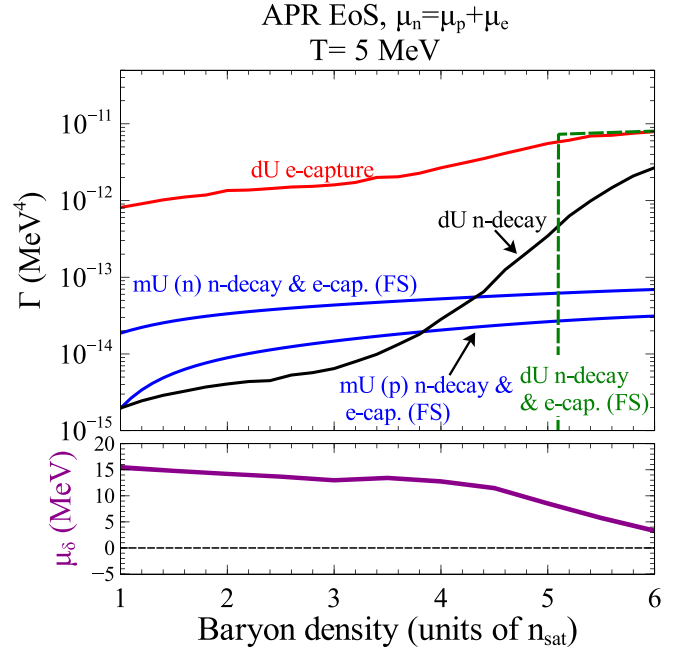
balance when μ_δ reaches its equilibrium value, which depends on the density and the temperature. This value of μ_δ at $T = 5$ MeV is shown in the bottom panel of Fig. 3. We see that, below the direct Urca threshold, μ_δ is about 15 MeV and it decreases but remains non-negligible above threshold as well.

In Fig. 4, we show, for several temperatures, the magnitude of the additional isospin-coupled chemical potential μ_δ needed to achieve true β equilibrium. At low temperatures, below 1 MeV, the standard criterion (2) is correct to within about 1 MeV; the only noticeable correction $\mu_\delta \approx 1.5$ MeV occurring right below threshold where direct Urca electron capture begins to dominate over modified Urca. After that, however, the correction term rises quickly with temperature: at $T = 5$ MeV we need $\mu_\delta \approx 15$ MeV and at $T = 10$ MeV we need $\mu_\delta \approx 23$ MeV. Although μ_δ drops with density once we reach the direct Urca threshold, that decrease becomes quite slow at these higher temperatures. If the neutrino-trapping temperature is indeed around 5 MeV (see Appendix A), then our calculations of μ_δ are only physically relevant at temperatures below 5 MeV. Above the neutrino-trapping temperature we expect that neutrinos are in statistical equilibrium with a chemical potential μ_ν obeying the detailed balance relation $\mu_n + \mu_\nu = \mu_p + \mu_e$.

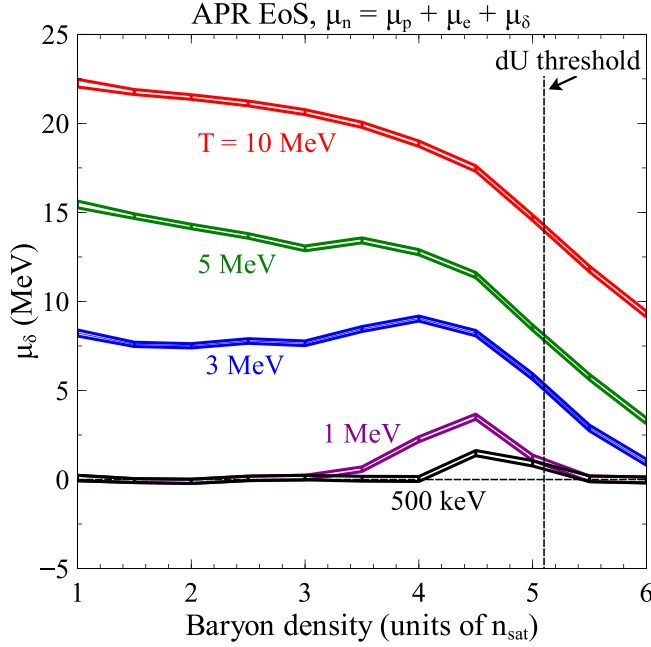The APR equation of state is based on variational calculations of the energy (as a function of density) of pure

FIG. 4. The isospin-coupled chemical potential μ_δ needed to achieve true β equilibrium in APR matter at various temperatures. For a given temperature, the upper and lower curves indicate the range of values of μ_δ that are consistent with our estimates of the theoretical uncertainty. Further details on the uncertainty are given in the text.
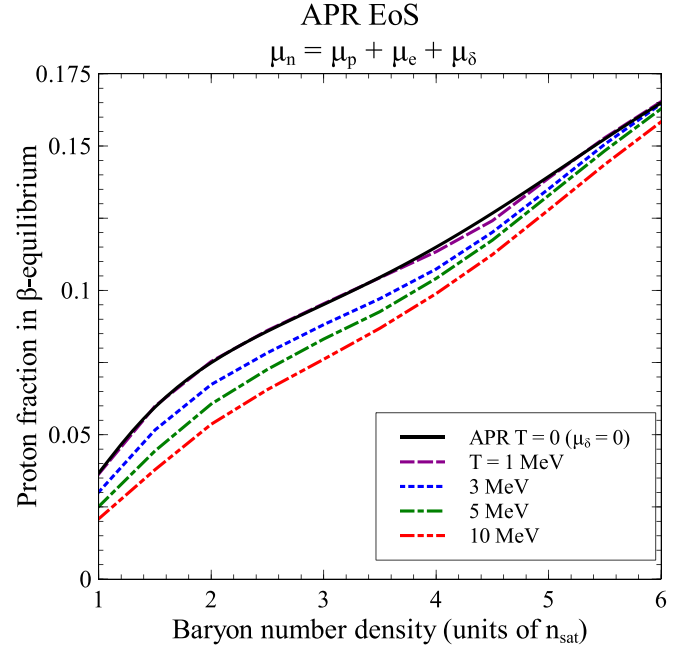

FIG. 5. Proton fraction in neutrino-transparent nuclear matter in true β equilibrium, for several different temperatures. As temperature increases, the β-equilibrated nuclear matter becomes more neutron-rich than predicted by the low-temperature β-equilibrium condition.

neutron matter (PNM, $x_p = 0$) and symmetric nuclear matter (SNM, $x_p = 0.5$). An interpolation scheme was used to get to the intermediate proton fraction, for a given density, that satisfies the low-temperature β-equilibrium condition (2) [27]. Thus, all thermodynamic quantities calculated within the APR framework are functions of both baryon density and proton fraction. To find the value of $\mu_\delta = \mu_n - \mu_p - \mu_e$ necessary to achieve true β equilibrium at a given density and temperature, we varied the proton fraction in discrete steps until we found a proton fraction at which there was net neutron production and an adjacent-step proton fraction at which there was net neutron destruction, giving us an upper and lower bound on μ_δ. These upper and lower bounds provide the theoretical error on μ_δ. The uncertainty in the direct Urca rate calculations, discussed at the end of Appendix C, is smaller than the binning of μ_δ, which is ≈ 300 keV.

The temperature-dependent correction μ_δ to the β-equilibrium condition arises from the temperature dependence of the proton fraction in true β equilibrium. In Fig. 5 we plot the proton fraction in true β equilibrium as a function of density, for various temperatures. As temperature rises above 1 MeV, the proton fraction drops. This reflects the predominance of electron capture over neutron decay seen in Fig. 3.

V. CONCLUSIONS

We have shown that that the standard low-temperature criterion (2) for β equilibrium breaks down in neutrino-transparent nuclear matter at densities above nuclear saturation density and temperatures above about 1 MeV. An additional isospin chemical potential (13) is required to obtain true equilibrium under the weak interactions. The ultimate reason for this is that neutrinos are not in thermal equilibrium, so the two reactions (1) that drive the system to equilibrium are not exact inverses of each other (neutrinos can only occur in final states) so the principle of detailed balance does not apply. Our calculations for nuclear matter obeying the APR equation of state show (Fig. 4) that the isospin chemical potential $\mu_\delta = \mu_n - \mu_p - \mu_e$ required to obtain β equilibrium becomes greater than about 5 MeV as the temperature rises above 1 MeV, and reaches a maximum value around 23 MeV at temperatures of 10 MeV.

We have recalculated the Urca rates for APR nuclear matter at $T = 5$ MeV in true β equilibrium. The results are given in Fig. 6, which shows that there are three processes that play the central role in β equilibration. Above threshold, direct Urca neutron decay balances with direct Urca electron capture. Far below threshold, n-spectator modified Urca neutron decay competes with direct Urca electron capture, but as threshold is approached from below, direct Urca neutron decay becomes increasingly important, eventually becoming more important than n-spectator modified Urca neutron decay.

In Fig. 7, we show the fractional change in the six direct Urca rates when the correct β-equilibrium condition is imposed, compared with the low-temperature criterion for β equilibrium (2). Far below threshold, the Urca rates increase or decrease by a factor of 10 and, far above threshold, the Urca rates approach their low-temperature β equilibrium (2) values.
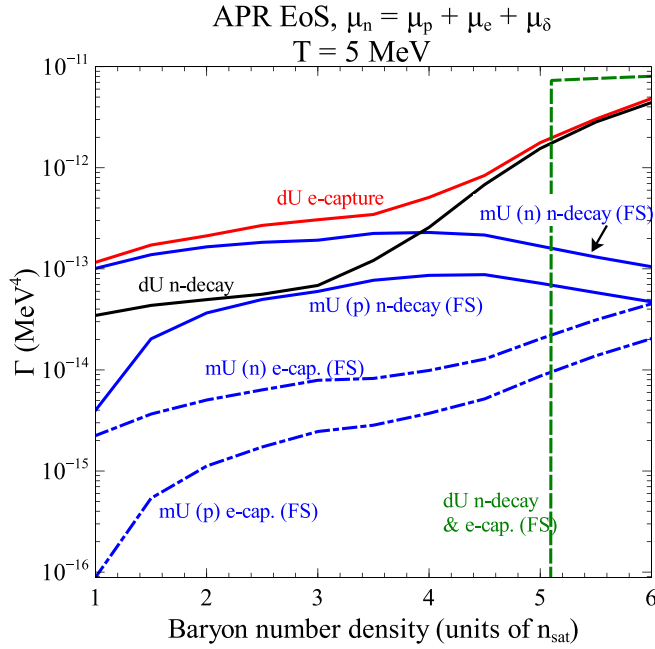
FIG. 6. Urca rates in true β equilibrium, $\mu_n = \mu_p + \mu_e + \mu_\delta$. Above threshold, the two direct Urca processes dominate. Below threshold, direct Urca electron capture balances against modified Urca neutron decay (n spectator) and, to a lesser extent, direct Urca neutron decay.

FIG. 7. Fractional change in the six Urca rates at $T = 5$ MeV when we change μ_δ from zero to the value for true β equilibrium. Below threshold, the change is the most prominent, and as density increases to far above the threshold density, the true β-equilibrium condition approaches the behavior of the low-temperature β-equilibrium condition (2).

The adjustment μ_δ to the low-temperature criterion for β equilibrium has implications for any effect stemming from weak interactions in β-equilibrated nuclear matter, in the temperature range from about 1 MeV to the neutrino trapping temperature. For example, the nuclear matter in neutron-star mergers, which certainly reaches such temperatures, undergoes significant density oscillations during the merger. The density oscillations may be damped by bulk viscosity, which arises from a resonance between the density oscillations and β equilibration of the proton fraction, which occurs via Urca processes [22,28,35]. The calculation of bulk viscosity relies on examining the adjustment of the neutron-decay and electron-capture rates as the nuclear matter is pushed out of β equilibrium so, if the criterion for β equilibrium is modified, it is likely that this will affect the calculated bulk viscosity for material in neutron-star mergers.

While we used the APR equation of state, which has two- and three-body nuclear interactions, to describe the nuclear matter in which the Urca processes take place, our calculation used the conventional Fermi–Dirac factors which assume that single-nucleon momentum eigenstates are also energy eigenstates. However, it is known [36] that short-range nucleon-nucleon interactions lead to a depletion of low-momentum states in the nucleon Fermi sea and a high-momentum tail above the Fermi surface, so a truly consistent calculation of the Urca rates would use modified Fermi–Dirac factors. Additionally, the fact that an energy eigenstate actually corresponds to a superposition of multi-particle–hole eigenstates
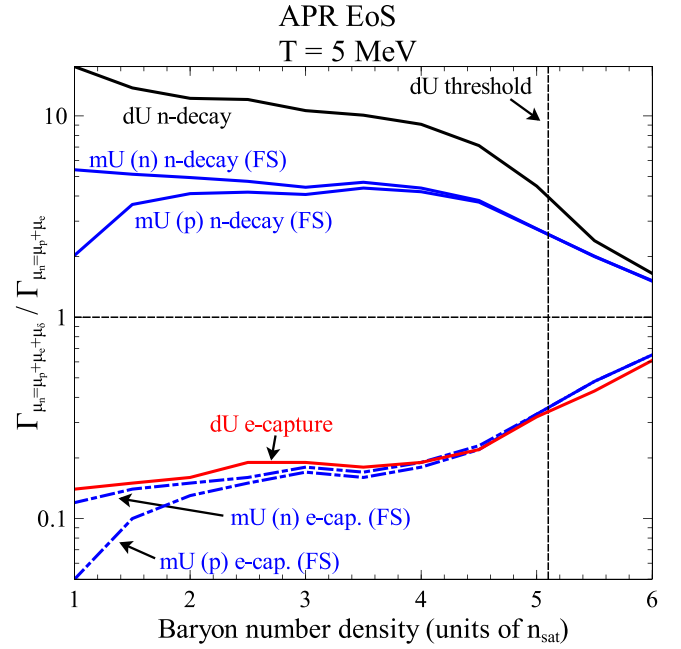
[17] could further blur the direct Urca threshold beyond the finite-temperature effects that we discuss in this paper.

In this work we did not consider particle processes involving muons, although the APR equation of state includes contributions from muons. Muons can participate in Urca processes and also in leptonic processes such as $\mu^- \rightarrow e^- + \bar{\nu}_e + \nu_\mu$. A complete treatment of the Urca processes in neutrino-transparent nuclear matter would introduce another chemical potential μ_f (which couples to lepton flavor, differentiating electrons from muons) whose value at a given temperature and density is determined by balancing the six muon Urca process rates.

APPENDIX A: NEUTRINO MEAN-FREE PATH

Our calculations are applicable to matter in which neutrinos are not trapped, which means our results are valid at temperatures up to the neutrino-trapping temperature for a neutron star. This is determined by the length of the neutrino mean-free path compared with the size of the star. The mean-free path depends on the neutrino energy and the temperature,
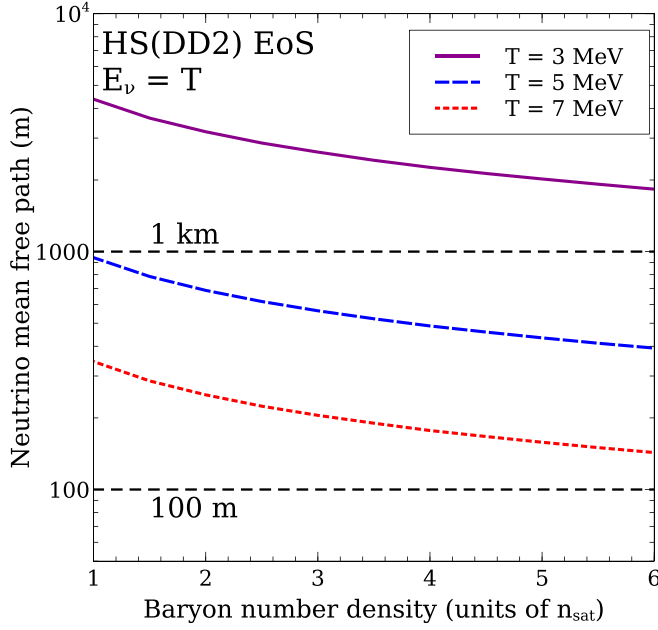
FIG. 8. Mean-free path of neutrinos in nuclear matter described by the HS(DD2) equation of state (EoS). As temperature rises above 5 MeV it becomes more likely that neutrinos will be trapped inside the merger region.

density, and composition of the nuclear matter with which it interacts. To get a reasonable idea of the neutrino-trapping temperature we used a start-of-the-art code developed in Refs. [18,19] and available online in Ref. [37] to calculate the neutrino mean-free paths due to charged and neutral current reactions in nuclear matter above nuclear saturation density. We used proton fractions and nuclear mean-field values from the HS(DD2) equation of state [38,39], which is tabulated online in Ref. [40]. The HS(DD2) equation of state is a relativistic mean-field theory consistent with most data from nuclear experiments and astrophysical constraints [41,42]. Unlike APR, it is tabulated for finite temperatures, making it suitable for estimating the temperature dependence of the mean-free path. The mean-free path for neutrinos with energy equal to the temperature is plotted in Fig. 8. We show the mean-free path for neutral-current neutrino-neutron scattering, since that is the dominant scattering process at densities above nuclear saturation density. At a temperature of 3 MeV, across the relevant range of densities, neutrinos always have a mean-free path of several kilometers, so they easily escape the merger region (whose radius is ≈ 10 km). At $T = 5$ MeV, the mean-free path varies from about 1 km at nuclear density down to 0.5 km at several times nuclear density, and at $T = 7$ MeV, the mean-free path is typically a few hundred meters. We conclude that it is reasonable to expect that neutrino trapping will only begin to become important when temperatures rise above 5 to 10 MeV.

APPENDIX B: MODIFIED URCA RATES WHEN $\mu_n \neq \mu_p + \mu_e$

We present here the Fermi-surface approximation of the modified Urca rates in nuclear matter which is out of

β-equilibrium (2) by an amount $\xi = (\mu_n - \mu_p - \mu_e)/T$. In the following expressions for the rates the nonequilibrium behavior is encapsulated in the function

$$
\begin{aligned}
F(\xi) = &-(\xi^4 + 10\pi^2\xi^2 + 9\pi^4)\text{Li}_3(-e^\xi) \\
&+ 12\xi(\xi^2 + 5\pi^2)\text{Li}_4(-e^\xi) - 24(3\xi^2 + 5\pi^2)\text{Li}_5(-e^\xi) \\
&+ 240\xi\text{Li}_6(-e^\xi) - 360\text{Li}_7(-e^\xi),
\end{aligned}
\tag{B1}
$$

where Li_n is the polylogarithm function of order n. We note that $F(0) \approx 2300$. The rate of modified Urca neutron decay with a neutron spectator is

$$
\begin{aligned}
\Gamma_{mU,nd(n)}(\xi) = &\frac{7}{64\pi^9} G^2 g_A^2 f_{\pi NN}^4 \frac{m_n^3 m_p}{m_\pi^4} \\
&\times \frac{p_{F_n}^4 p_{F_p}}{(p_{F_n}^2 + m_\pi^2)^2} F(\xi)\vartheta_n T^7,
\end{aligned}
\tag{B2}
$$

where ϑ_n is defined as in Eq. (12). The rate of modified Urca electron capture with a neutron spectator is

$$
\Gamma_{mU,ec(n)}(\xi) = \Gamma_{mU,nd(n)}(-\xi),
\tag{B3}
$$

and so the two n-spectator modified Urca rates agree in low-temperature β equilibrium (2). The Fermi-surface approximation of the modified Urca neutron decay process with a proton spectator is

$$
\begin{aligned}
\Gamma_{mU,nd(p)}(\xi) = &\frac{1}{64\pi^9} G^2 g_A^2 f_{\pi NN}^4 \frac{m_n m_p^3}{m_\pi^4} \\
&\times \frac{p_{F_n}(p_{F_n} - p_{F_p})^4}{[(p_{F_n} - p_{F_p})^2 + m_\pi^2]^2} F(\xi)\vartheta_p T^7,
\end{aligned}
\tag{B4}
$$

with ϑ_p defined as in Eq. (13), and the modified Urca electron-capture rate with a proton spectator is

$$
\Gamma_{mU,ec(p)}(\xi) = \Gamma_{mU,nd(p)}(-\xi),
\tag{B5}
$$

where again both modified Urca rates with a p spectator agree in low-temperature β equilibrium (2).

APPENDIX C: EXACT DIRECT URCA RATE INTEGRAL

The neutron-decay rate given by a twelve-dimensional integral in Eq. (6) can be reduced, without approximation, to a three-dimensional integral. Integrating over neutrino three-momentum, we have

$$
\begin{aligned}
\Gamma_n = &\frac{G^2}{128\pi^8} \int d^3p_n\, d^3p_p\, d^3p_e\, f_n(1 - f_p)(1 - f_e) \\
&\times \delta(q - |\mathbf{p}_n - \mathbf{p}_p - \mathbf{p}_e|) \\
&\times \left(1 + 3g_A^2 + (1 - g_A^2)\hat{\mathbf{p}}_e \cdot \frac{\mathbf{p}_n - \mathbf{p}_p - \mathbf{p}_e}{|\mathbf{p}_n - \mathbf{p}_p - \mathbf{p}_e|}\right),
\end{aligned}
\tag{C1}
$$

where we define $q \equiv E_n - E_p - E_e$, and the "hat" denotes a unit vector. We adopt spherical coordinates for the momentum of each of the three particles. We have the freedom to choose the coordinates such that the neutron momentum lies along the z axis, and the proton momentum lies in the same plane as the neutron momentum, and so the momentum unit vectors

are written as

$$\hat{\mathbf{p}}_n = (0, 0, 1), \tag{C2}$$

$$\hat{\mathbf{p}}_p = \left(\sqrt{1 - z_p^2}, 0, z_p\right), \tag{C3}$$

$$\hat{\mathbf{p}}_e = \left(\sqrt{1 - z_e^2}\cos\phi, \sqrt{1 - z_e^2}\sin\phi, z_e\right), \tag{C4}$$

where z_p and z_e are cosines of the polar angles of the proton and electron momenta and as such, take values from -1 to 1. The azimuthal angle ϕ of the electron with respect to the

plane formed by the proton and neutron momenta ranges from 0 to 2π.

This choice of coordinates allows us to integrate over the three trivial angles, giving a factor of $8\pi^2$. The rate integral can now be written as

$$\Gamma_n = \frac{G^2}{16\pi^6} \int_0^\infty dp_n \, dp_p \, dp_e \, p_n^2 p_p^2 p_e^2$$
$$\times f_n (1 - f_p)(1 - f_e) I(p_n, p_p, p_e), \tag{C5}$$

where

$$I = \int_{-1}^{1} dz_e \int_{-1}^{1} dz_p \int_0^{2\pi} d\phi \, \delta\left(q - \sqrt{p_n^2 + p_p^2 + p_e^2 + 2p_p p_e \sqrt{1 - z_p^2}\sqrt{1 - z_e^2}\cos\phi + 2p_p p_e z_p z_e - 2p_n p_p z_p - 2p_n p_e z_e}\right)$$

$$\times \left(1 + 3g_A^2 + \left(1 - g_A^2\right)\frac{p_n z_e - p_p z_p z_e - p_e - p_p\sqrt{1 - z_p^2}\sqrt{1 - z_e^2}\cos\phi}{\sqrt{p_n^2 + p_p^2 + p_e^2 + 2p_p p_e\sqrt{1 - z_p^2}\sqrt{1 - z_e^2}\cos\phi + 2p_p p_e z_p z_e - 2p_n p_p z_p - 2p_n p_e z_e}}\right). \tag{C6}$$

We do the ϕ integral first, using the δ function. Clearly we require $q > 0$, because if q is negative, the argument of the δ function could never be zero and thus the integral would be zero. For $q > 0$, the δ function argument vanishes for either zero or two values of ϕ between 0 and 2π. We find that

$$I = 4|q| \int_{-1}^{1} dz_p \left[1 + 3g_A^2 + \frac{1 - g_A^2}{2p_e q}\left(p_n^2 + p_p^2 - p_e^2 - q^2 - 2p_n p_p z_p\right)\right]\Theta(q)$$

$$\times \int_{-1}^{1} dz_e \frac{1}{\sqrt{4p_p^2 p_e^2\left(1 - z_p^2\right)\left(1 - z_e^2\right) - \left(q^2 - p_n^2 - p_p^2 - p_e^2 - 2p_p p_e z_p z_e + 2p_n p_p z_p + 2p_n p_e z_e\right)^2}}\Theta(B), \tag{C7}$$

where the step function $\Theta(B)$ enforces $B > 0$, where

$$B = 2p_p p_e \sqrt{1 - z_p^2}\sqrt{1 - z_e^2} - |q^2 - p_n^2 - p_p^2 - p_e^2 - 2p_p p_e z_p z_e + 2p_n p_p z_p + 2p_n p_e z_e|. \tag{C8}$$

This is the condition for there to be two, not zero, values of ϕ in the integration range which make the argument of the δ function vanish and thus contribute to the integral.

We now evaluate the z_e integral, noting that the step function $\Theta(B)$ adjusts the range of integration. Only if $C > 0$, where

$$C = 2p_e|q| - |p_e^2 + q^2 - p_n^2 - p_p^2 + 2p_n p_p z_p|, \tag{C9}$$

is the step function nonzero for any range of z_e in the interval $[-1, 1]$, in which case the step function is nonzero only for $z_e^- < z_e < z_e^+$, where $z_e^\pm$ lie inside the interval $[-1, 1]$, and thus $z_e^\pm$ become the new integration bounds. Doing the z_e integral, we find

$$I = \frac{2\pi|q|}{p_e}\Theta(q) \int_{-1}^{1} dz_p \, \Theta(C)\left(\frac{1 + 3g_A^2 + \frac{1 - g_A^2}{2p_e q}\left(p_n^2 + p_p^2 - p_e^2 - q^2 - 2p_n p_p z_p\right)}{\sqrt{p_n^2 + p_p^2 - 2p_n p_p z_p}}\right). \tag{C10}$$

The step function $\Theta(C)$ creates a restriction on the bounds of z_p and so the actual range of integration over z_p is the intersection of the intervals $[-1, 1]$ and $[z_p^-, z_p^+]$, where $z_p^\pm = (p_n^2 + p_p^2 - p_e^2 - q^2 \pm 2p_e|q|)/(2p_n p_p)$, and so the range of integration will depend on the values of $\{p_n, p_p, p_e\}$. Evaluating the integral over z_p with the bounds y^+ and y^-, we have

$$I(p_n, p_p, p_e) = \frac{2\pi|q|}{p_n p_p p_e}\Theta(q) J(p_n, p_p, p_e) \tag{C11}$$

where

$$J(p_n, p_p, p_e) = \left[\left(1 + 3g_A^2 - (1 - g_A^2)\frac{p_e^2 + q^2}{2p_e q}\right)y^{1/2} + \frac{1 - g_A^2}{6p_e q}y^{3/2}\right]\Bigg|_{y=y^-}^{y=y^+}, \tag{C12}$$

with

$$
y^+ = \begin{cases}
(p_e + |q|)^2 & \text{if } -1 < z_p^- < 1 < z_p^+ \\
(p_e + |q|)^2 & \text{if } -1 < z_p^- < z_p^+ < 1 \\
(p_n + p_p)^2 & \text{if } z_p^- < -1 < 1 < z_p^+ \\
(p_n + p_p)^2 & \text{if } z_p^- < -1 < z_p^+ < 1,
\end{cases} \quad \text{(C13)}
$$

and

$$
y^- = \begin{cases}
(p_n - p_p)^2 & \text{if } -1 < z_p^- < 1 < z_p^+ \\
(p_e - |q|)^2 & \text{if } -1 < z_p^- < z_p^+ < 1 \\
(p_n - p_p)^2 & \text{if } z_p^- < -1 < 1 < z_p^+ \\
(p_e - |q|)^2 & \text{if } z_p^- < -1 < z_p^+ < 1.
\end{cases} \quad \text{(C14)}
$$

Thus, the direct Urca neutron decay rate is

$$
\Gamma_n = \frac{G^2}{8\pi^5} \int_0^\infty dp_n \, dp_p \, dp_e \, p_n p_p p_e |q| \Theta(q)
$$
$$
\times f_n(1 - f_p)(1 - f_e) J(p_n, p_p, p_e), \quad \text{(C15)}
$$

with $J(p_n, p_p, p_e)$ as defined in Eqs. (C12)–(C14).

The direct Urca electron-capture rate integral is identical, except that $f_n(1 - f_p)(1 - f_e)$ is replaced by $(1 - f_n)f_p f_e$ and, because the neutrino is now on the same side of the reaction as the neutron, instead of with the electron and proton, $\Theta(q)$ is replaced by $\Theta(-q)$.

The remaining three-dimensional integral in Eq. (C15) can be done numerically (we used *Mathematica*'s Monte Carlo integration routine), giving the direct Urca rate results shown in Figs. 2 and 3. *Mathematica*'s estimated error on the numerical integrals is under 20%, and repeated evaluation of the integrals leads to results within 10% of their average.

---

[1] D. Yakovlev, O. Gnedin, M. Gusakov, A. Kaminker, K. Levenfish, and A. Potekhin, Neutron star cooling, Nucl. Phys. A **752**, 590 (2005).

[2] D. G. Yakovlev and C. J. Pethick, Neutron star cooling, Annu. Rev. Astron. Astrophys. **42**, 169 (2004).

[3] E. F. Brown, A. Cumming, F. J. Fattoyev, C. J. Horowitz, D. Page, and S. Reddy, Rapid Neutrino Cooling in the Neutron Star MXB 1659-29, Phys. Rev. Lett. **120**, 182701 (2018).

[4] B. P. Abbott *et al.*, Multi-messenger observations of a binary neutron star merger, Astrophys. J. Lett. **848**, L12 (2017).

[5] B. P. Abbott *et al.* (LIGO Scientific Collaboration and Virgo Collaboration), GW170817: Observation of Gravitational Waves from a Binary Neutron Star Inspiral, Phys. Rev. Lett. **119**, 161101 (2017).

[6] L. Baiotti and L. Rezzolla, Binary neutron-star mergers: A review of Einstein's richest laboratory, Rep. Prog. Phys. **80**, 096901 (2016).

[7] S. Bernuzzi, D. Radice, C. D. Ott, L. F. Roberts, P. Mösta, and F. Galeazzi, How loud are neutron star mergers? Phys. Rev. D **94**, 024023 (2016).

[8] D. Radice, F. Galeazzi, J. Lippuner, L. F. Roberts, C. D. Ott, and L. Rezzolla, Dynamical mass ejection from binary neutron star mergers, Mon. Not. R. Astron. Soc. **460**, 3255 (2016).

[9] L. Baiotti, B. Giacomazzo, and L. Rezzolla, Accurate evolutions of inspiralling neutron-star binaries: Prompt and delayed collapse to a black hole, Phys. Rev. D **78**, 084033 (2008).

[10] R. Oechslin, H.-T. Janka, and A. Marek, Relativistic neutron star merger simulations with non-zero temperature equations of state - I. Variation of binary parameters and equation of state, Astron. Astrophys. **467**, 395 (2007).

[11] K. Kiuchi, Y. Sekiguchi, M. Shibata, and K. Taniguchi, Long-term general relativistic simulation of binary neutron stars collapsing to a black hole, Phys. Rev. D **80**, 064037 (2009).

[12] A. Endrizzi, R. Ciolfi, B. Giacomazzo, W. Kastaun, and T. Kawamura, General relativistic magnetohydrodynamic simulations of binary neutron star mergers with the APR4 equation of state, Class. Quantum Grav. **33**, 164001 (2016).

[13] A. Bauswein, H. T. Janka, and R. Oechslin, Testing approximations of thermal effects in neutron star merger simulations, Phys. Rev. D **82**, 084043 (2010).

[14] K. Hotokezaka, K. Kyutoku, H. Okawa, M. Shibata, and K. Kiuchi, Binary neutron star mergers: Dependence on the nuclear equation of state, Phys. Rev. D **83**, 124008 (2011).

[15] F. Maione, R. De Pietri, A. Feo, and F. Loffler, Binary neutron star merger simulations with different initial orbital frequency and equation of state, Class. Quantum Grav. **33**, 175009 (2016).

[16] S. Reddy, M. Prakash, and J. M. Lattimer, Neutrino interactions in hot and dense matter, Phys. Rev. D **58**, 013009 (1998).

[17] S. Reddy, M. Prakash, J. M. Lattimer, and J. A. Pons, Effects of strong and electromagnetic correlations on neutrino interactions in dense matter, Phys. Rev. C **59**, 2888 (1999).

[18] L. F. Roberts and S. Reddy, Charged current neutrino interactions in hot and dense matter, Phys. Rev. C **95**, 045807 (2017).

[19] L. F. Roberts, S. Reddy, and G. Shen, Medium modification of the charged-current neutrino opacity and its implications, Phys. Rev. C **86**, 065803 (2012).

[20] See Supplemental Material at http://link.aps.org/supplemental/10.1103/PhysRevC.98.065806 for tabulated data presented in our figures.

[21] S. L. Shapiro and S. A. Teukolsky, *Black Holes, White Dwarfs, and Neutron Stars: The Physics of Compact Objects* (Wiley, Hoboken, New Jersey, 1983).

[22] D. Yakovlev, A. Kaminker, O. Gnedin, and P. Haensel, Neutrino emission from neutron stars, Phys. Rep. **354**, 1 (2001).

[23] J. M. Lattimer, C. J. Pethick, M. Prakash, and P. Haensel, Direct URCA Process in Neutron Stars, Phys. Rev. Lett. **66**, 2701 (1991).

[24] D. G. Yakovlev and K. P. Levenfish, Modified URCA process in neutron star cores, Astron. Astrophys. **297**, 717 (1995).

[25] Y.-F. Yuan, Electron-positron capture rates and a steady state equilibrium condition for an electron-positron plasma with nucleons, Phys. Rev. D **72**, 013007 (2005).

[26] M.-Q. Liu, Steady state equilibrium condition of npe$^\pm$ gas and its application to astrophysics, Res. Astron. Astrophys. **11**, 91 (2011).

[27] A. Akmal, V. R. Pandharipande, and D. G. Ravenhall, The equation of state for nucleon matter and neutron star structure, Phys. Rev. C **58**, 1804 (1998).

[28] M. G. Alford, L. Bovard, M. Hanauske, L. Rezzolla, and K. Schwenzer, Viscous Dissipation and Heat Conduction in Binary Neutron-Star Mergers, Phys. Rev. Lett. **120**, 041101 (2018).

[29] L. Villain and P. Haensel, Non-equilibrium β processes in superfluid neutron star cores, Astron. Astrophys. **444**, 539 (2005).

[30] P. Haensel, K. P. Levenfish, and D. G. Yakovlev, Bulk viscosity in superfluid neutron star cores. I. Direct Urca processes in $npe\mu$ matter, Astron. Astrophys. **357**, 1157 (2000).

[31] A. D. Kaminker, D. G. Yakovlev, and P. Haensel, Theory of neutrino emission from nucleon–hyperon matter in neutron stars: Angular integrals, Astrophys. Space Sci. **361**, 267 (2016).

[32] B. L. Friman and O. V. Maxwell, Neutron star neutrino emissivities, Astrophys. J. **232**, 541 (1979).

[33] P. Haensel, K. P. Levenfish, and D. G. Yakovlev, Bulk viscosity in superfluid neutron star cores - II. Modified Urca processes in $npe\mu$ matter, Astron. Astrophys. **372**, 130 (2001).

[34] D. T. Son and M. A. Stephanov, QCD at Finite Isospin Density, Phys. Rev. Lett. **86**, 592 (2001).

[35] M. G. Alford, S. Mahmoodifar, and K. Schwenzer, Large amplitude behavior of the bulk viscosity of dense matter, J. Phys. G **37**, 125202 (2010).

[36] A. Rios, A. Polls, and W. H. Dickhoff, Depletion of the nuclear Fermi sea, Phys. Rev. C **79**, 064308 (2009).

[37] L. Roberts and S. Reddy, https://bitbucket.org/lroberts/nuopac/src (2016).

[38] M. Hempel and J. Schaffner-Bielich, Statistical model for a complete supernova equation of state, Nucl. Phys. A **837**, 210 (2010).

[39] S. Typel, G. Ropke, T. Klahn, D. Blaschke, and H. H. Wolter, Composition and thermodynamics of nuclear matter with light clusters, Phys. Rev. C **81**, 015803 (2010).

[40] M. Hempel, https://astro.physik.unibas.ch/people/matthias-hempel/equations-of-state.html (2018).

[41] T. Fischer, M. Hempel, I. Sagert, Y. Suwa, and J. Schaffner-Bielich, Symmetry energy impact in simulations of core-collapse supernovae, Eur. Phys. J. A **50**, 46 (2014).

[42] M. Oertel, M. Hempel, T. Klahn, and S. Typel, Equations of state for supernovae and compact stars, Rev. Mod. Phys. **89**, 015007 (2017).